Union College
Union | Digital Works

Honors Theses   Student Work

6-2017

Triboelectric Turbines: Design and Construction of a Multi-Rotor Counter-Rotating Wind Turbine Utilizing Direct-Current Triboelectric Nanogenerators

Adam Forti
Union College - Schenectady, NY

Follow this and additional works at: https://digitalworks.union.edu/theses

Part of the Energy Systems Commons

Triboelectric Turbines:

Design and Construction of a Multi-Rotor,

Counter-Rotating Wind Turbine Utilizing

Direct-Current Triboelectric Nanogenerators

By

Adam Forti

❉ ❉ ❉

Submitted in partial fulfillment

of the requirements for

Honors in the Department of Mechanical Engineering

UNION COLLEGE

March, 2017

ABSTRACT

FORTI, ADAM: Triboelectric Turbines: Design and Construction of a Multi-Rotor, Counter-Rotating Wind Turbine Utilizing Direct-Current Triboelectric Nanogenerators. Deparment of Mechanical Engineering, March 2017.

ADVISOR: Rebecca Cortez, Ph.D.

Direct-current triboelectric nanogenerators (DC-TENG) harness the friction generated between dissimilar rotating materials and convert it to useable electrical power. One of the many potential applications of this technology is in small scale renewable energy. A wind turbine was designed in which multiple DC-TENG generators would be attached to turbine blades of varying dimensions. This project involved the design and construction of several rotating DC-TENG prototypes, followed by measuring the electrical output of each nanogenerator at various rotational speeds.

Table of Contents

Table of Figures

Introduction

Triboelectric Nanogenerators

Recently, the development of triboelectric nanogenerators (TENG) has enabled an alternative method of harvesting mechanical energy from the environment [1]. These devices make use of the triboelectric effect, the tendency of a material to gain or lose electrons when it is forced against another material. Materials which are more positive on the triboelectric scale have a tendency to lose electrons when in contact with other materials, and those which gain electrons are more negative on the triboelectric scale. This tendency is quantified as the charge affinity (nC/J), which corresponds to one nanoampsec/wattsec of friction [2]. Two insulators from opposite ends of the triboelectric series produce the largest charge distribution when they are pressed together and separated. A few selected materials are shown in Table 1, with the full table included in Appendix A.

Table 1 – Selected materials and triboelectric charge affinity. The metal effect indicates the charge acquired by the material if rubbed with metal, relative to the normal affinity. In this column, N indicates Normal (or consistent with the standard affinity) and W indicates a weak resulting charge affinity. Tests were performed by Bill Lee (Ph.D., physics). ©2009 by AlphaLab, Inc. (TriField.com), which also manufactured the test equipment used [2]. Full table included in Appendix A.

Insulator Name	Affinity (nC/J)	Metal Effect
Polyurethane foam	+60	+N
Box sealing tape (BOPP)	+55	+W
Hair, oily skin	+45	+N
Solid polyurethane, filled	+40	+N
Glass (soda)	+25	+N
Cotton	+5	+N
Nitrile rubber	+3	-W
Wool	0	-W
Polycarbonate	-5	-W
ABS	-5	-N
Polystyrene	-70	-N
PVC (rigid vinyl)	-100	-N
Butyl rubber, filled	-135	-N
Teflon	-190	-N

Triboelectric materials have been tested for functionality in various configurations, the fundamental difference being the mode of separation of two dissimilar materials [1]. Typically, one is an insulator near one extreme of the triboelectric series, and the other material is a conductor. Periodic vertical displacement has produced a peak AC current density of 16 mA/m^2, which relies on the pressing and lifting of an external force to generate electricity [3, 4]. Alternative designs make use of single-electrode, freestanding triboelectric-layer, and contact-sliding modes of TENG [3]. All of these designs lead to an alternating current (AC) output, as the triboelectric materials are repeatedly contacted and separated. Although this can be measured and used to sporadically illuminate arrays of lights, the practical use of these technologies for energy storage is limited by their dependence on including a voltage rectifier to produce a direct current (DC) output, which leads to considerable energy waste [1].

Direct-Current Triboelectric Nanogenerators

Further refinements within contact-sliding modes of triboelectronics by Zhang et al. have led to rotating configurations which allow the TENG to produce a DC current, leading to the designation DC TENG [1]. Multiple layers of aluminum and polyvinyl chloride (PVC) are cut into specific, radially symmetric patterns containing either one or multiple segments. When arranged in the configuration shown in Figure 1, and spun by an external power source, they can produce power because, when in contact, the PVC attracts electrons from the aluminum. The arrangement of the carbon fiber brushes and layers of materials enables a DC output, as the aluminum electrode rotates relative to the polyvinyl chloride (PVC) insulator. This cycle can be summarized as shown in Figure 2.
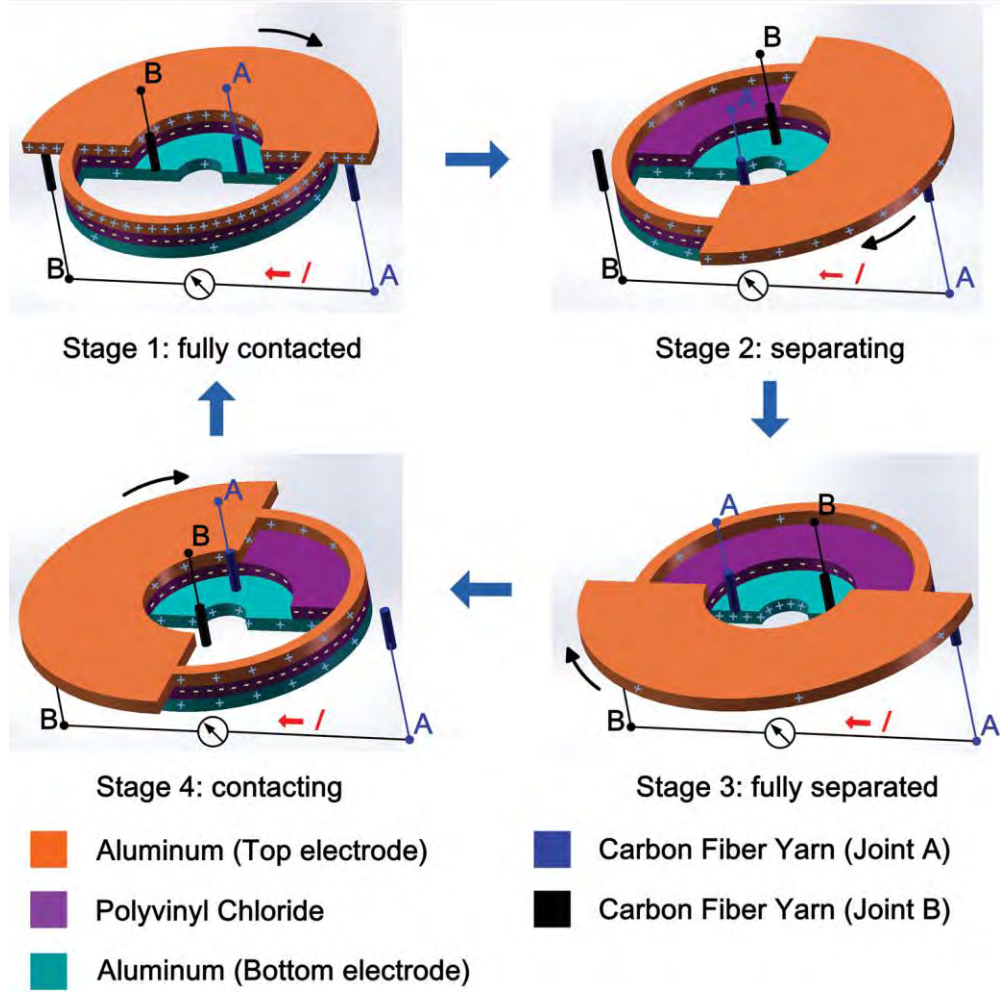
Figure 1: Operation of the semi-circle DC TENG. Image courtesy of Zhang et al [1].

Stage 1
- **Maximum Potential Energy**
- Triboelectric effect has already forced electrons from aluminum into PVC.

Stage 2
- **Power Output**
- Rotation reduces contact area, allowing electrons to flow through Joint A (due to voltage difference). This causes a current from Joint A through the load to Joint B.

Stage 3
- **Minimum Potential Energy**
- Connections to Joints A and B switch.

Stage 4
- **Triboelectric Charging**
- Rotation increases contact area, forcing electrons to move from the aluminum to PVC (due to triboelectric effect).

Stage 1
- **Maximum Potential Energy**
- Connections to Joints A and B switch.

Figure 2: Summary of events which occur during a single cycle of a DC TENG, as shown in Figure 1.

This outline is based on the assumption that the PVC and the bottom electrode are electrically the same the entire time, which is a weak assumption. In reality, the bottom electrode would always be more positive than the PVC (due to triboelectric effect). In essence, this may indicate that the PVC-bottom electrode junction acts somewhat like a one-way electron gate, similar to the concept of a PNP bipolar junction transistor. This possibility is conjecture, and not explored further in this report.

The success of these designs introduces a variety of options for triboelectric energy harvesting applications wherever rotational mechanical energy exists. The simplest of these DC-TENG designs is the semi-circle, shown in Figure 1, above. It has a single segment of aluminum, and will be alternatively referred to as an s1 DC TENG. This device was found to produce a power density of 25 mW/m^2 while operating at 750 RPM, where the area of interest is the contact area between the top electrode and polyvinyl chloride in Figure 1 [1].

The equivalent circuit diagrams for the various stages are shown in Figure 3a. Modifications on the semi-circle design are shown in Figure 3b, increasing the number of electrode segments while maintaining the same total surface area of electrodes. Figure 3c shows an eighth-circle DC-TENG assembly (an s4 DC TENG) with a diameter of 2.4 inches, to provide a sense of scale.
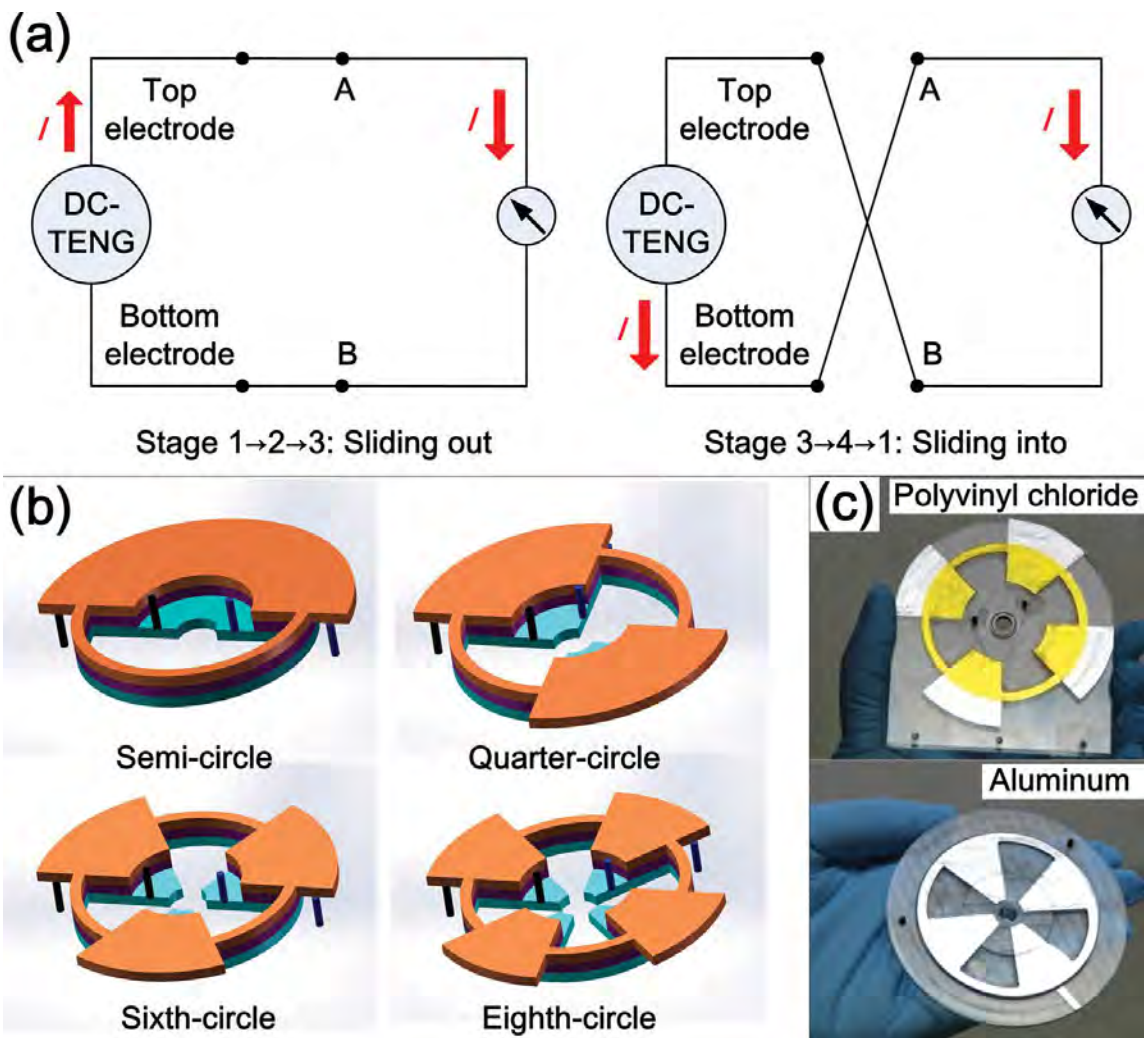
Figure 3: (a) The equivalent circuits during one full rotation of the semi-circle DC-TENG. (b) CAD model of various alternative designs. (c) Actual eighth-circle DC-TENG, including the carbon brushes. The outer diameter of the aluminum circle is 2.4 inches. Image courtesy of Zhang et al [1].

When tested over a range of rotational speeds from 150 to 1350 RPM, the designs with the higher number of segments had significantly faster increases in short circuit current density.

Similarly, an increase in rotational speed led to an increase in the short circuit current density [1]. From these analyses, the optimal design of DC-TENG rotates rapidly and consists of as many electrode segments as possible.

Anticipated Generator Output

Predictions for the output current of DC TENG were made based on the reported results in the literature. Zhang et al. determined linear relationships between short circuit current density (J_{sc}, in mA/m^2) and rotating speed (RPM), with an increase in number of segments corresponding to an increase in the slope of that curve [1]. They include data from s1, s2, s3, and s4 DC TENG (referred to as Semi, Quarter, Sixth, and Eighth, respectively, in their publication). The data is reproduced in Figure 4, which also includes the extrapolated prediction for short circuit current density for the s20 DC TENG (which would be labelled Fortieth by Zhang et al.).
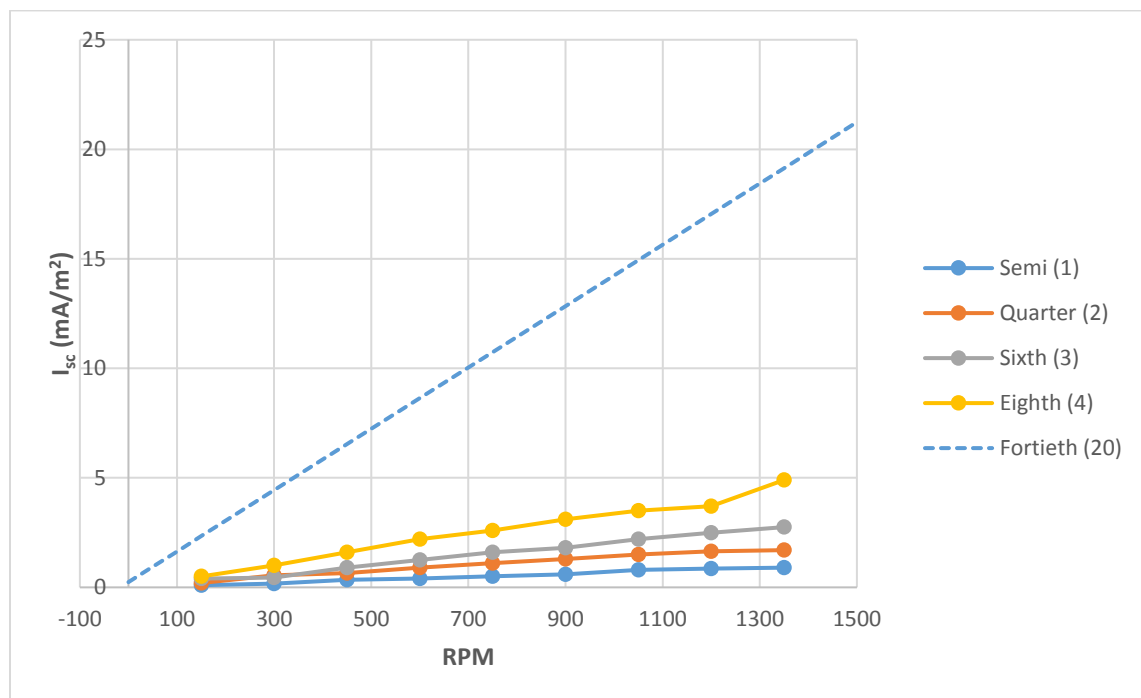
Figure 4: Reproduced data from Zhang et al. and extrapolated prediction (shown with dashed line) for the short circuit current density of a DC TENG at various rotational speeds [1].

The extrapolation was obtained by first dividing the short circuit current density of each of the data sets from Zhang by the corresponding number of segments, producing the dataset shown in Figure 5. This data was found to fit a linear best fit line, shown as Equation 1. The resulting R^2 value of 0.94 is sufficiently accurate for this approximation. The speed in revolutions per minute (RPM) was substituted into this equation, and the result multiplied by the number of segments (20 for the s20 design). This product is the extrapolated data shown in Figure 4.
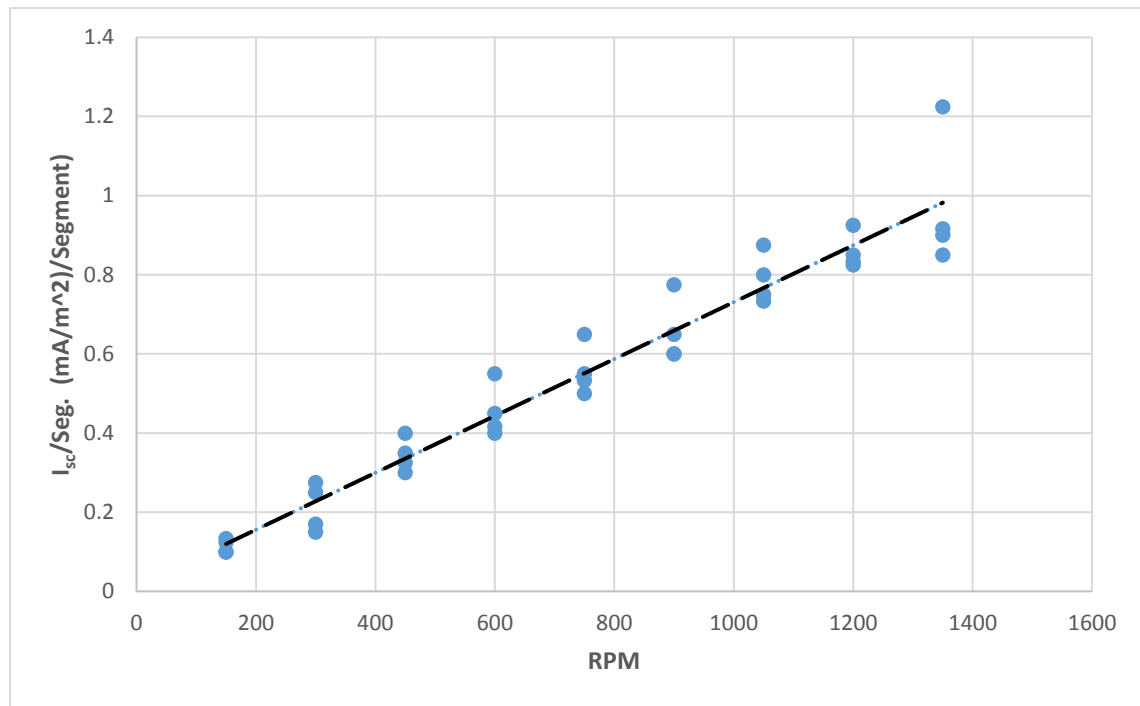
Figure 5: Short circuit current from Zhang et al. DC TENG divided by the number of segments within each generator at various rotational speeds [1]. The linear best fit line is as Equation 1.

$$\left(\frac{I_{SC}}{Seg.}\right) = 0.0007 * (RPM) + 0.012 \qquad\qquad 1$$

The slope of Equation 1 is likely to be somehow indicative of some property inherent to either a particular triboelectric material, friction between triboelectric layers, DC TENG in general, or some other aspect of these nanogenerators. It is also possible that the assumed linear fit is inaccurate, or only applies to a limited range of rotational speeds. These unknown aspects of this curve are not explored further in this report, but may be well worth further investigation.

Turbines

The design of wind turbines has been a focus of environmental engineers for many years, and there are many designs which can easily translate the energy of incoming wind into rotational energy though both vertical axis wind turbines (VAWT) and horizontal axis wind turbines (HAWT) [5]. Traditional turbines utilize a single rotor that spins perpendicular to incoming wind, and this rotation spins a generator, producing electricity. This is where it is necessary to consider the Betz limit, which states that up to 59% of wind power can ever be harnessed by a turbine [5]. To produce large amounts of power despite this limitation, these designs benefit from massive turbines moving at high speeds.

Rotating DC-TENG technology could be fastened to the rotor of a traditional windmill, with one layer fixed to the axle, producing electricity through the triboelectric effect. However, this technology becomes more effective with increased speed, suggesting the use of smaller turbines. These would produce less torque than a massive HAWT, but can still operate quickly. In addition, placing a second rotor on the same axis and reversing the blade orientation will allow the adjacent rotors to spin in opposite directions. A DC TENG placed with one layer on each rotor would experience much greater relative rotational speed from the same incident wind due to this counter-rotation. If the rotors can be designed to be sufficiently light, a series of rotors of increasing size can be placed on a single axis. The resulting turbine has the potential to generate a substantial amount of electricity, depending primarily on the efficiency of the DC TENG and the efficiency of the blade airfoils.

The state of California conducted a study of a counter-rotating wind turbine system, which utilizes two rotors spinning opposite directions on the same turbine tower. Each turbine spins a separate portion of the generator, leading to an increased efficiency of up to 40% at low

wind speeds. In addition to the resulting power increase, this moment-balancing design reduced the bending stress on the supporting tower compared to a single rotor system [6]. Such counter-rotating turbines cannot utilize more than two rotors, as there are only two elements of a traditional generator that rotate opposite one another. Other multi-rotor designs make use of a backup rotor to "catch" the air flow deflected from a front rotor, leading to increased overall efficiencies [7]. However, at this time, there have been no attempts to functionalize the rotational DC-TENG for energy harvesting using a turbine of any kind, let alone a turbine with multiple rotors.

Materials and Methods

Materials

This senior design project is intended to result in the production of a direct-current triboelectric nanogenerator which can be used by an ongoing Green Fee project to produce electric power from low speed winds on campus at Union College [8]. The majority of the structural components were laser cut from 0.25-inch thick acrylic sheets purchased from McMaster Carr. Electronic slip rings and motors were purchased from Pololu. PVC, polycarbonate, and aluminum sheet were purchased from McMaster-Carr, and machined using a water jet in the Union College machine shop. Short sections of pipe and bushings were precision machined by technicians in this shop as well. Acetyl butyl styrene (ABS) filament was purchased from MatterHackers and used to 3D print model turbine blades.

Design and Manufacture of DC TENG Models

Sanity Check: Model 1

The first product was model 1.1, a simple arrangement in which a scrap of acrylic was covered with a sheet of aluminum foil, which was then taped in place, as shown in Figure 6. The

foil was rubbed rapidly against a scrap of polyvinyl chloride for approximately 10 seconds, at which point the materials were separated. The voltage difference between the aluminum and ground was measured immediately, and a temporary voltage spike was measured. Although this voltage quickly dissipated, it was the first visible indication that the triboelectric effect may result in measurable output power.
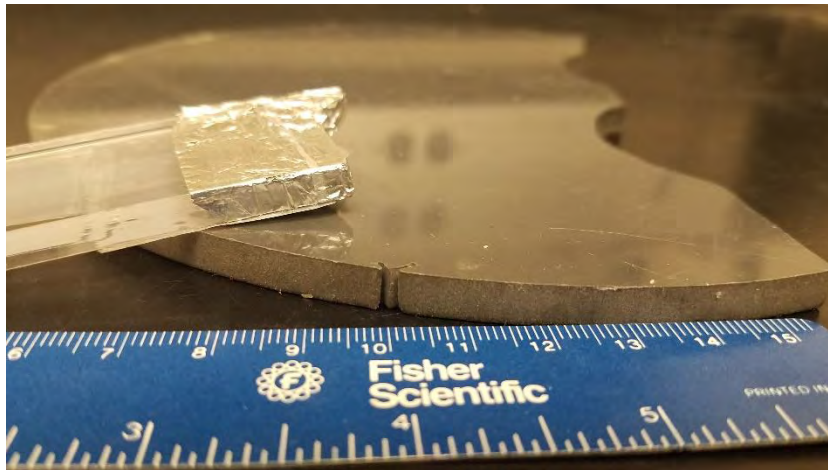
Figure 6: Test model used to confirm the effects of triboelectricity. Acrylic (clear) is approximately 0.25 inches thick and 1 inch wide.

First Test: Model 2

A more complicated model was constructed when funds became available. It was designed such that one section of the DC TENG could be rotated with respect to the other by means of a small DC motor, as shown in Figure 7. Two iterations of DC TENG were designed for this test section, with model 2.1 a replica of the one-segment design (referred to as s1) shown in the literature, and model 2.2 having twenty segments (s20). The diameters of each of these DC-TENG, measured as the exterior diameter of the PVC component, were 2.5 inches.
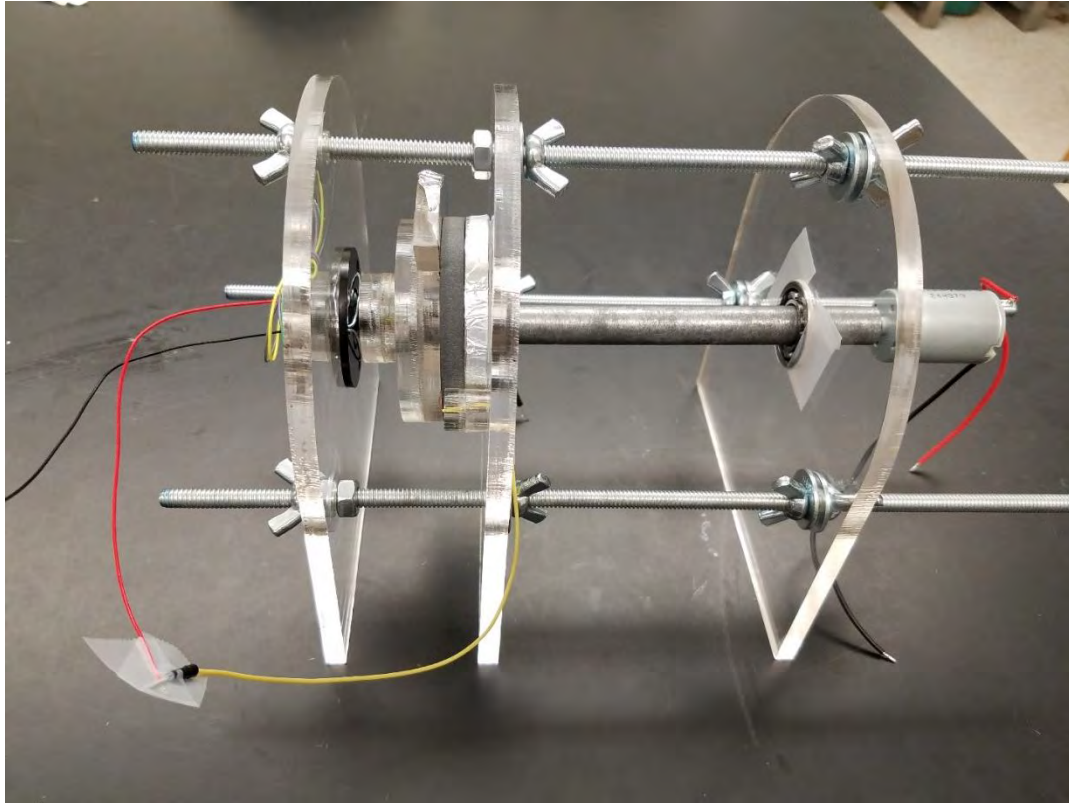
Figure 7: DC TENG test model 2.1. The s1 generator has a diameter of 2.5 inches, measured as the outer diameter of the PVC component.

Although this model was capable of producing some measureable output, it was too small to enable testing of more complicated DC TENG with higher segment counts. When attempted, the electric brushes would be in contact with multiple segments simultaneously, preventing power generation.

Second Test: Model 3

Model 3.1 was built to be a considerably larger and more useable test stand than the previous system, and capable of testing two DC-TENG simultaneously. In this model, the axis of the DC TENG is stationary while the central portion (the rotor) spins freely, which more closely imitates the actual system in use within a wind turbine. Model 3.2, shown in Figure 8, implemented several improvements on the design of model 3.1, most notably the addition of a motor and supporting structures which enabled the rotor to be tested. Both DC TENG in model

3.2 were s20 designs with PVC outer diameters of 8 inches. As is apparent in this image, on one side of the rotor the narrow electrode (no external tabs) is fixed to the test stand, while on the opposite end the wide electrode (multiple external tabs) is fixed to the test stand. These sides are described as the Narrow Electrode Fixed (NEF) and Wide Electrode Fixed (WEF) sides of the rotor, respectively.
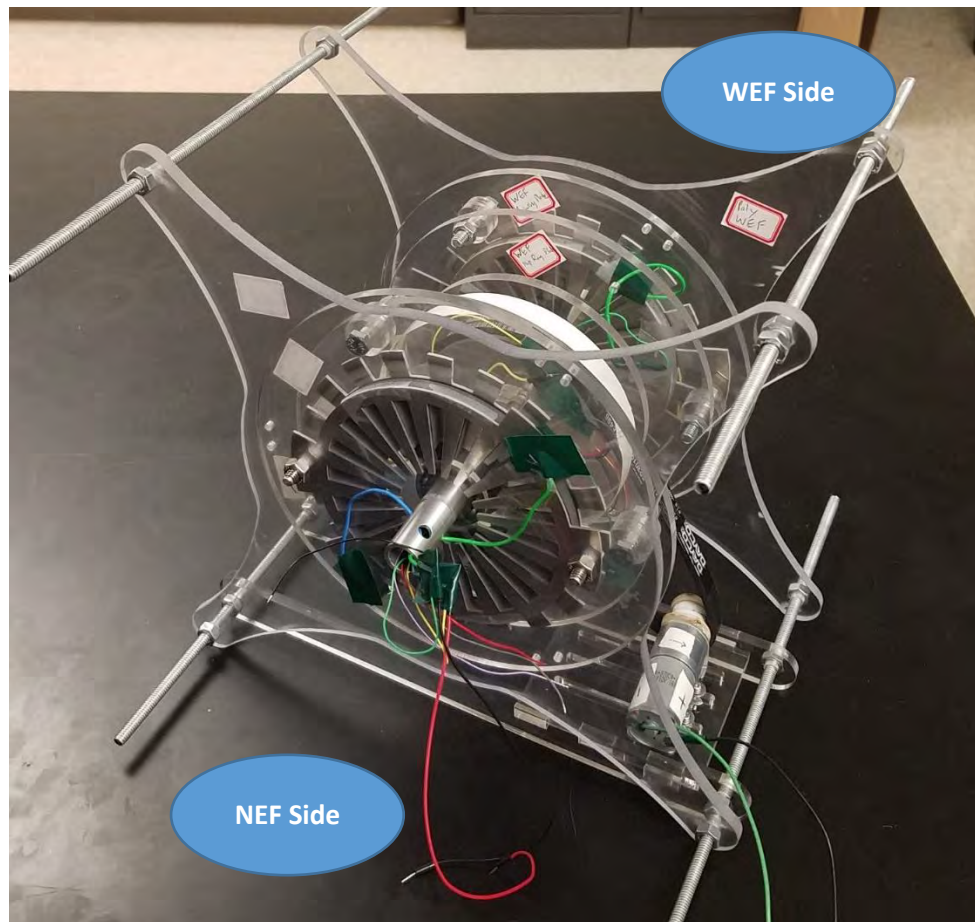
Figure 8: DC TENG test model 3.2, containing a single rotor with two electrically independent s20 generators. The rotor is driven through a belt drive system mounted on the test stand.

A detailed diagram of model 3.2 is shown in Figure 9. Key components of the assembly are labeled corresponding to entries in Table 2. A full list of components is provided in Appendix B. Additional views of the CAD model are available in Appendix C.
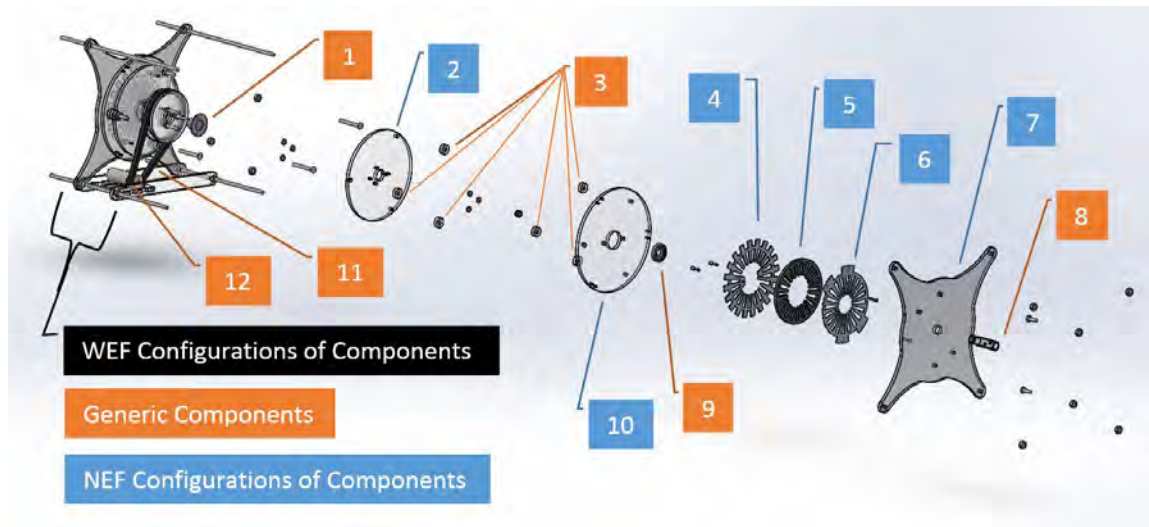
Figure 9: Exploded view of DC TENG model 3.2, with key components labeled. Only key generic components and those designed specifically for the Narrow Electrode Fixed (NEF) half of the apparatus are labelled. Full component list shown in Appendix B.

Table 2: Part list corresponding to the labels in Figure 9. Full component list shown in Appendix B.

Label	Part Name	Material	Part Description
1	Slip Ring with Flange	Plastic/wiring	6 wires, max 240V @ 2A
2	Slip Ring Connection Plate NEF	0.25-inch acrylic	Laser Cut by Engineering Tech.
3	Spacing Washer	0.25-inch acrylic	Laser Cut by Engineering Tech.
4	Wide Electrode s20 NEF	0.063-inch aluminum sheet	Water Jet by Machine Shop
5	PVC s20	0.25-inch	Water Jet by Machine Shop
6	Narrow Electrode s20 NEF	0.063-inch aluminum sheet	Water Jet by Machine Shop
7	Stand Cap NEF	0.25-inch polycarbonate	Water Jet by Machine Shop
8	Axial Pipe	Schedule 40 aluminum size $^3/_8$	Machined by Machine Shop
9	Ball Bearing	stainless steel	5/8" Shaft Dia., 1-3/8" OD
10	Turbine Cap NEF	0.25-inch acrylic	Laser Cut by Engineering Tech.
11	Drive Belt	Rubber	Dayco ELA V-Rubber Belt
12	Gear Motor	Metal	47:1 Gear Ratio

Although the turbine blades were not constructed for this model, they were designed to be located as shown in Figure 10. This version would be used for testing either in specific locations outdoors or, if scaled down to an appropriate size, in a wind tunnel.
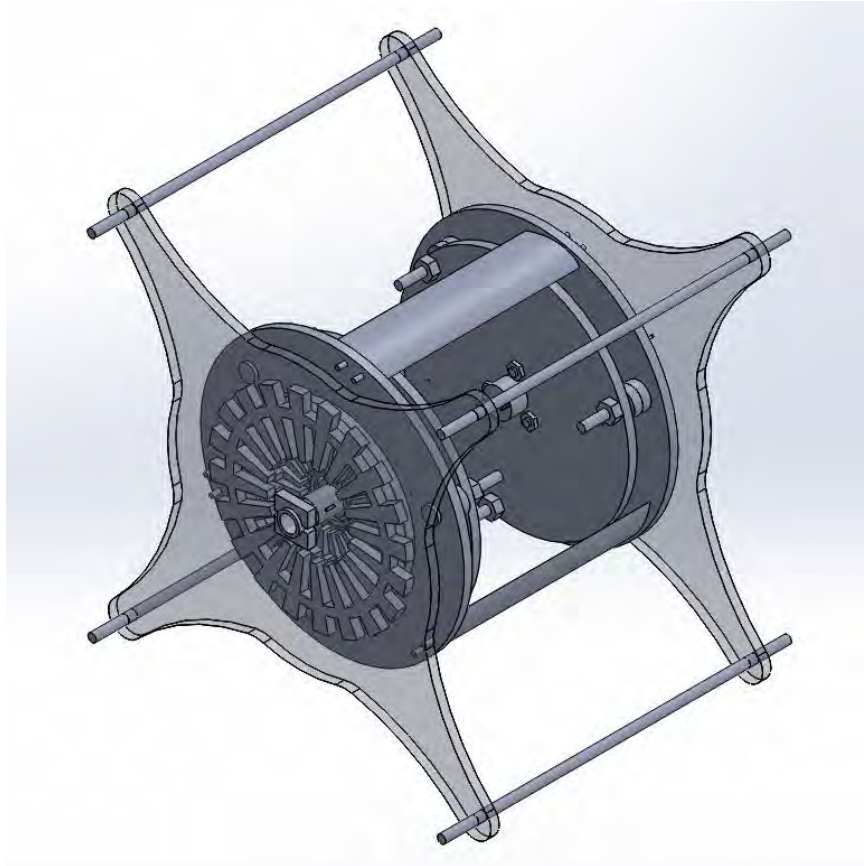
Figure 10: Version of model 3.2 in which the belt drive system has been removed and turbine blades added. Ultimately, this intended to be the basic design for models used in wind tunnel testing.

Future Design: Model 3.3

Although time did not permit its fabrication, model 3.3 was designed to enable three DC TENG to be tested simultaneously. A computer-aided design (CAD) model is shown in Figure 11, in which turbine blades have been added to show the intended final configuration. This model would be too large to test in the on-campus wind tunnel, requiring the use of a high powered fan and an anemometer instead. Such tests have not yet been designed fully.
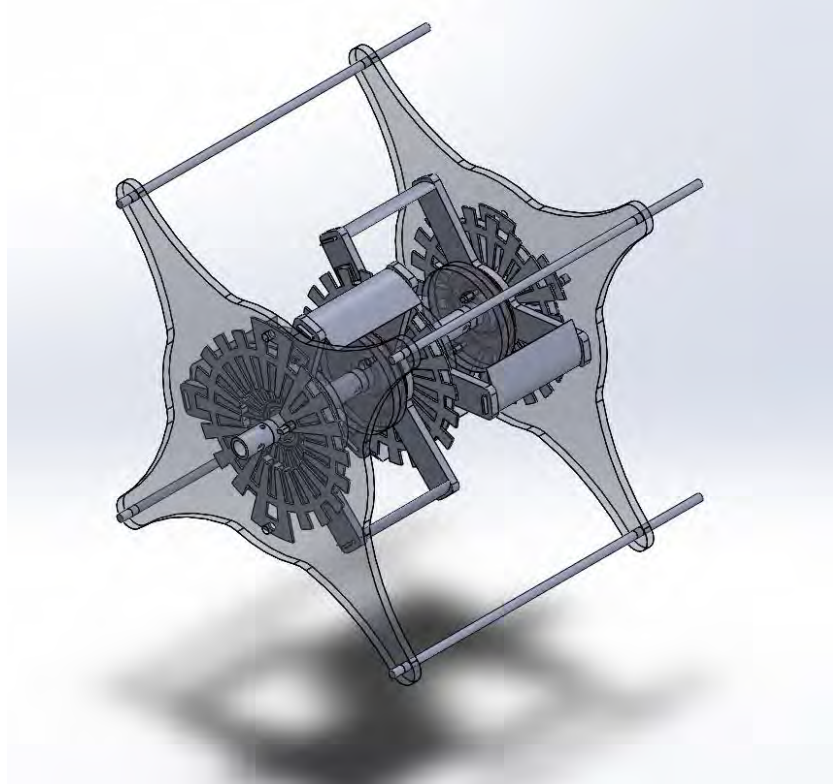
Figure 11: SolidWorks model of multiple-rotor DC TENG test stand model 3.3. Note the opposite orientation of turbine blades on each rotor.

This model would be tested with each rotor spinning in the opposite direction, as they would in a multi-rotor wind turbine array. Counter-rotation would be due to switching the orientation of each set of turbine blades. For this model, the first iteration of the blades were 3D printed from acetyl butyl styrene (ABS) based on a design obtained from airfoilplotter.com.

Figure 12: Turbine blades, manufactured through additive manufacturing (3D printing).

Testing of Model 3.2

The experimental setup was designed to evaluate the open circuit voltage output of each DC TENG within model 3.2. One oscilloscope channel was dedicated to each DC TENG, with one probe attached to each output wire. The following MATLAB script was used to collect the data from both oscilloscope channels and display each in a separate figure plotting voltage vs time:

```
clc, clear
[signal1, time1] = swave(1);
[signal2, time2] = swave(2);
```

The code used here uses the function "swave," written by John Spinelli (Union College Department of Computer and Electrical Engineering), which creates an independent figure displaying the readout from the screen of the oscilloscope for each channel. The screen range is easily adjustable, and limiting the field of view of the oscilloscope limits the data range while increasing the accuracy of each measurement. Regardless of the time span, the code saves 600 data points at equal time increments. During testing, the DC motor and belt drive assembly were directly wired to an adjustable laboratory power supply, and used to spin the center portion of the assembly (the rotor). A handheld tachometer was used to measure the rotations per minute of the rotor, which were constant at a given power input into the motor. When a steady speed was attained, the MATLAB code was initialized, and data acquired.

A nearly identical setup was used to measure an approximation of short circuit current, in which the two output wires of a DC TENG were connected across a low-resistance (R, in Ohms [Ω]) resistor. The resulting voltage difference (V, in volts [V]) would be used to calculate the current (I, in amperes [A]) using Ohms Law, shown in Equation 2.

$$V = I * R \hspace{4cm} 2$$

Testing Results and Discussion

Open Circuit Voltage of Model 3.2

The voltage output for a single DC TENG within model 3.2 is shown in Figure 13, with each data set corresponding to a test run at a different rotational speed. Within each of the figures generated by the open circuit voltage tests, the datasets were vertically shifted so that multiple could be displayed in the same plot. Each follows a general pattern of having the majority of data points approximately equal to zero, with periodic voltage spikes. It was initially thought that these spikes were noise from the system, as they were highly irregular, but it was found to be due to mechanical irregularities which forced brushes to only make contact intermittently. Upon repairing this issue, a regular pattern emerged due to the radial symmetry of the electrode geometry (which is the source of the electrons comprising the current flow). The frequency of peaks corresponds to the frequency at which a single segment of the DC TENG would be expected to pass by a stationary point (which is the frequency of completed DC TENG cycles, as described by Figures 1 and 2).
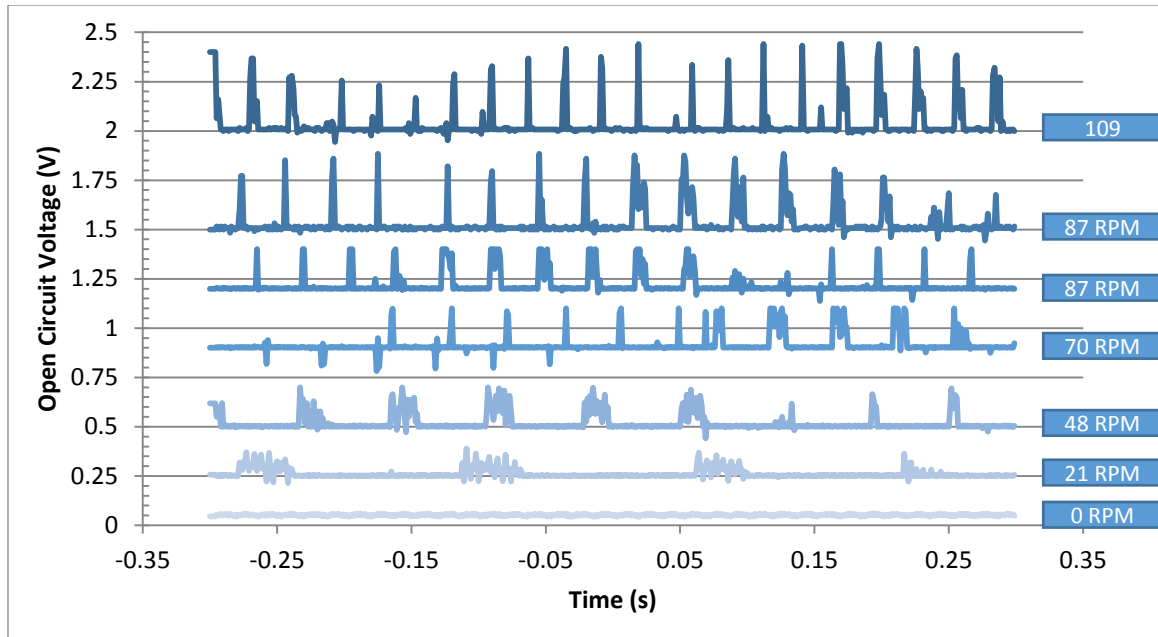
Figure 13: Open circuit voltage of a single DC-TENG at various rotational speeds, as indicated by the accompanying blocks on the right of the figure. Each data set contains a nearly uniform horizontal line which corresponds to a reading of zero volts, to elucidate analysis each was offset by a different amount. The proportionate difference between each peak and the baseline for that data set is preserved.

Critically, the consistent orientation of the voltage spikes is a strong indicator that the desired direct current output was produced (when any energy was being produced at all). In other tests, the voltage spikes are largely negative. This is solely due to the arrangement of the channel probes, and would switch sign if these probes were reversed. In the figure, as the rotational speed increased, so too did the frequency and magnitude of the voltage spikes produced by the DC-TENG. Although the maximum output was only between 0.1 V to 0.4 V, this data was only collected at speeds up to 109 RPM, Zhang et al. performed tests between 150 and 1350 RPM [1]. At increased speeds, the energy production is expected to be much greater, increasing linearly [1].

Short Circuit Current of Model 3.2

Short circuit current density, obtained by dividing the output current of a DC TENG by the effective surface area (defined as the surface area of a single face of the PVC layer), is the primary

method used by Zhang et al. to characterize the output of the DC TENG [1]. Attempts to measure the voltage drop across a resistance of 330 Ω resulted in negligible voltage readings, indicating that the current was extremely low. Lower-resistance resistors must be obtained and arranged in parallel to reduce the overall resistance and enable actual values to be calculated for the short circuit current.

Efficiency Approximations

There are multiple measures of efficiency for a DC TENG turbine. First, the DC TENG efficiency can be defined as the energy output by the DC TENG divided by energy of the rotating mass as it spins. For a driven test turbine, such as model 3.2, the motor efficiency is the energy of the rotating mass as it spins divided by the electrical energy forced into the motor. For a wind tunnel test turbine, such as the thus far unbuilt model 3.3, the turbine blade efficiency is the energy of the spinning mass divided by the energy of the wind (for wind energy approximation, see Appendix D). This is limited by the Betz Limit, which fixes the maximum turbine blade efficiency at 59% [5]. Finally, the overall turbine efficiency would be the energy of the impinging wind divided by the energy produced by the DC TENG.

The energy of the rotating mass can be calculated from its angular velocity (ω, in radians/s) and a computer-based calculation of the mass moment of inertia (J in kg*m^2), shown in Equation 3.

$$E_{rot} = \frac{1}{2} * J * \omega^2 \qquad\qquad 3$$

An evaluation of the mass properties of the rotating mass in model 3.2, highlighted in Figure 14 below, calculated the mass moment of inertia about the axis of rotation to be 21.4 lb*in^2 (see Appendix E for additional calculations).
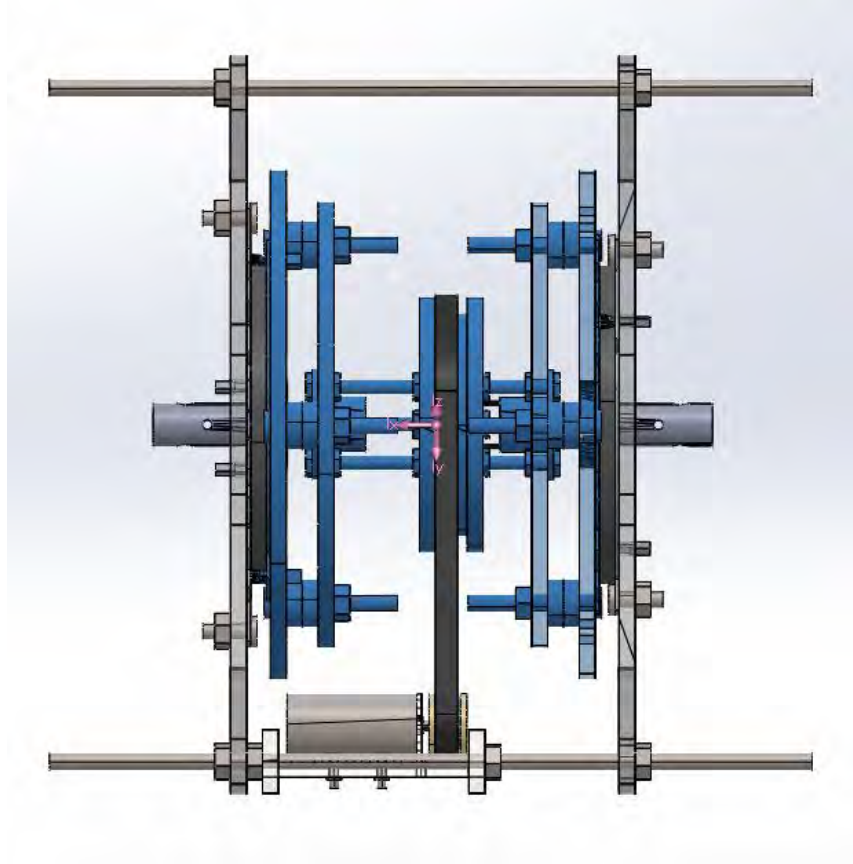
Figure 14: Side view of model 3.2, in which the rotating components have been highlighted in blue as part of the mass property calculation provided in Appendix E. The ink axis shown are located at the center of mass of the selection, with Ix oriented along the axis of rotation.

Using Equation 3, the kinetic energy of the rotating section at various angular speeds was

calculated, and the results are listed in Table 3.

Table 3: Calculated kinetic energy of rotating components at rotational speeds tested previously.

RPM	Kinetic Energy (J)
21	0.02
48	0.08
70	0.18
87	0.26
109	0.41

Typically, the energy produced by the DC TENG can be calculated by the measured output,

multiplying the power produced by time. From this, the efficiency of the DC TENG would be

determined. However, due to the lack of data for output current, this energy cannot be calculated at this time.

Future Work

Green Fee Project

This project was intended to produce a proof of concept DC TENG prototype for use in a wind turbine, and as a result there are multiple areas which remain to be explored in the future. As part of an ongoing Green Fee project, more extensive electrical testing will be completed, with priority going to short circuit current measurements and open circuit voltage measurements over a wide range of rotational speed [8]. This short circuit current, when divided by the effective surface area to produce short circuit current density, will be directly comparable to the data produced by Zhang et al., as discussed above. In addition, an array of these prototypes with varying diameters will be tested in vertical and horizontal orientations. Thinner sheets of PVC will be used to reduce weight and improve electrical conductivity between it and the aluminum layers. A DC TENG with 10 segments will be constructed and compared to the current model to confirm the effects of segmentation number. The success of the Green Fee project also requires an understanding of the effects of electrical configuration between multiple DC TENG, as at present, it is unknown if wiring DC TENG together in series or in parallel will have an impact on the underlying phenomena. It is necessary to complete a more thorough characterization of the present design's DC output before the combination of multiple generators can be explored further.

Independent Research

In addition to the steps which will be completed in the short term, there are many areas which may be improved through focused design projects. These include improving the brush design, studying the effect of using conductive lubricants (such as graphite), studying the effects of surface roughness, optimizing the number of segments, optimizing the thickness of the triboelectric layers, and replacing the PVC layer with one of Teflon or other triboelectric materials, based on their relative triboelectric values (see Appendix A). Beyond the improvement of individual DC TENG, it will be necessary to make improvements in how arrays of DC TENG rotors will operate together. This may include optimizing the pressure between generators, investigating wear prevention, and calculating the tradeoff between having more DC TENG and using a longer blade length to make occupy the same volume. Ultimately, as the technology is integrated into wind turbines, it will be necessary to calculate the cost of production per kWh achieved by these turbines, and compare to that of typical wind turbines. I believe that this technology has the potential to reduce the capital required significantly, leading to a reduced payoff period, which is critical to eventually making this technology viable.

Utilization

As this project transitions into the Green Fee project, the objective shifts to constructing a fully functional wind turbine composed of several arrays, each containing multiple DC TENG [8]. Such a device must have a purpose, and when discussing how the turbine will be used, several factors must be considered.

Directly connecting the turbine to the electrical grid would require conversion from DC to AC current (reducing the power output), significant paperwork, and a large installation cost. Instead, the DC output of the turbine can be directly used to charge a bank of batteries. This stores

the variable power output of the turbine in a readily avaiable, easily controlled form. These batteries can then be used to directly power other devices, such as lights or drinking fountains (which would require the batteries to be permanently wired to these devices). Alternatively, the batteries can be physically removed from the charging array one at a time, and used to power other objects (such as golf carts or portable electronics). Clearly, the power output of the turbine determines which of these forms is the most practical. Also of primary importance is the accesibility of the battery bank, which is dependant on the location of the actual wind turbine.

Proper location is absolutely critical for this project. Wind speed, safety, accessibility, aesthetics, administrative approval, and other factors will all need to be taken into account when making this choice. In general, higher elevations above ground level directly corellate with higher wind speeds, and rather than construct a one-hundred foot turbine, it is much more practical to build an approximately 10 foot turbine on top of an existing, multistory building. At the moment, the Union College administration has expressed a commitment to maintaining the historical appearance of the main campus, which makes it unlikely that approval would be granted for such locations as the roof of the Peter Irving Wold Center, the roof of Reamer Campus Center, along the wall near the flagpole in the center of campus, or other potentially suitable locations (as determined by technical factors such as typical wind speed). Safety considerations support the use of rooftops, as this would prevent people or objects from colliding with the turbine without necessitating the addition of a safety cage. Rooftops do make installation, operation and maintenance somewhat more complicated and potentially dangerous, though there are several accessible roofs on campus that eliminate these risks. One such potential site may eventually be found on or near the new Science and Engineering Center, presently under construction. Accessibility is especially important if the design proves to require extensive maintenance, or if the power is collected in batteries which are intended to be removed for use.

If the final turbine is calculated to produce below 1 W, it would not be sufficient to power a small light up display, and would have no appreciable impact on the carbon footprint of the college. In this case the remainder of the Green Fee funds may be invested in continuing to improve the technology, and not manufacturing a full scale turbine.

If the final turbine would produce between 1 W and 250 W, it is not enough energy to be of practical use to the college. However, it could be used to trickle charge battery packs or illuminate a light emmitting diode (LED) array. In this case there are several options. If the installation costs allow, it could be beneficial to install several turbines near one another, which will work in tandem. These could have rotors which are either the same size or of varying sizes, which would enable multiple optimal wind speeds of operation for the set of turbines.

If a single turbine (or a collection of several turbines) can produce at least 250 W, it will be enough to assist with charging much larger batteries [9]. This could be useful for supplementing the power needed to operate Union-owned electric carts or other vehicles, to power a phone charging station, or many other possibilities. This scenario provides the most flexibility as far as utilization options, and is clearly the ideal case, as well as the least likely.

If economic and manufacturing considerations allow, installing multiple turbines of varying geometries would lead to increased overall power output and potentially an wider range of operational wind speeds. As outlined above, if the turbines are capable of producing even just a small amount of power at low wind speed, there are several options for utilizing their output.

Lessons Learned

The majority of lessons learned over the course of this project were developed as solutions to very specific practical problems, while others were much more broadly applicable.

- Research First
  - Search the internet for related ideas to ensure others have not already done the same thing
  - Read technical papers – including patents – to develop a more thorough understanding of underlying phenomena and methodologies
  - Quantify the desired scope of your project, and evaluate its ultimate "worth" to you to ensure you will remain motivated throughout the process
- Measure critical material properties beforehand
  - Adhesives are typically insulators, so should not be relied upon to conduct electricity
  - Some materials cannot be machined using specific techniques
- Design for manufacturing
  - Be specific in dimensions, tolerances, file and part names, and materials
  - Never indicate "take your time" to machinists, they will not
  - Concentrate complexity into unique parts so you do not need to modify standard parts
  - Large pieces are difficult to keep perfectly flat
  - Occasionally, the cost of standard parts is prohibitive because they are manufactured at a high quality, and it is more cost effective to build your own stand in component
  - Design flexibility into select components which can be adjusted as desired
- Balance rigidity and manufacturability
  - Tight tolerances can make construction difficult or permanent
  - Loose tolerances produce loose joints which can wobble and get looser as a result
  - Avoid non-locking nuts and threaded rods
  - Recognize that nuts on spinning objects will either loosen or tighten, depending on direction of rotation
- Share your ideas
  - Getting people interested keeps you excited about your project and committed to its success
  - When people know what you are doing, they may make suggestions which would never have occurred to you otherwise
  - Asking for help from professionals (professors, machinists, technicians, farmers, students, etc.) can lead to new ideas and new partners in your endeavor
  - Exposing your ideas to criticism and questions helps you move beyond your self-imposed limits
- Keep careful notes
  - Take pictures and videos at every step
  - Save files in multiple locations
  - Carefully label everything
  - Use consistent and intuitive naming system

- o Keep track of where you make mistakes
- o Plan all expenditures in advance and track spending
- o Preserve all receipts and images of all receipts
- Plan ahead
  - o Avoid calling internationally unless you are equipped to do so
  - o Search throughout physical or online stores for items similar in form to what you are looking for, as there may be unexpected products available which solve your problem
  - o Start early prototyping with small models that are cheap to manufacture
  - o Do not rely on 3D printing to be rapid or successful
  - o Organize tests so that failure can be educational
  - o Account for lead times and hidden fees when ordering materials
- Prioritize long term goals
  - o Design components so they may be easily modified in digital and physical form
  - o Label such that multiple iterations will be easily traceable
  - o Determine which design changes bring you closer to your goal and which will need to be replaced in the next iteration regardless

Conclusion

At present, the characterization of model 3.2 is largely incomplete, making any conclusions about the effectiveness of the current design premature. However, it is evident that the conceived design has been successful in producing a measurable direct current voltage while running at relatively slow angular velocities. In addition, the technology was easily scaled and extrapolated from the designs previously published, indicating that for future improvements it may be similarly simple to adjust and scale various features as needed. It remains to be seen whether the design will become effective enough to be integrated into wind turbines, however, the potential for direct-current triboelectronic nanogenerators is apparent.

References

[1] Zhang, Chi, Tao Zhou, Wei Tang, Changbao Han, Limin Zhang, and Zhong Wang Lin. "Rotating-Disk-Based Direct-Current Triboelectric Nanogenerator." *Advanced Energy Materials* 4 (2014): n. pag. Materials Views. Web. Aug. 2016.

[2] Lee, Bill. "The TriboElectric Series." *AlphaLab Inc*. N.p., 2009. Web. Sep. 2016.

[3] Wang, Zhong. "Triboelectric nanogenerators as new energy technology and self-powered sensors – Principles, problems and perspectives." *Faraday Discussions* (2014): n. pag. Royal Society of Chemistry. Web. Jun. 2016.

[4] Wang, Sihone, Lin, Long, and Zhong Lin Wang. "Nanoscale Triboelectric-Effect-Enabled Energy Conversion for Sustainably Powering Portable Electronics." *Nano Letters* 12 (2012): 6339-6346. ACS Publications. Web. Jun. 2016.

[5] "The Betz Limit." PelaFlow Consulting. Web. Nov. 2016. <http://www.wind-power-program.com/betz.htm>

[6] Mitchel III, David. "Counter Rotating Wind Turbine System." (2003) State of California Energy Commission. Web. Sep. 2016.

[7] Stobart, Andrew Ferrand, Wind Turbine Resource Conservation Plc, assignee. Patent WO1992012343 A1. 23 July 1992. Web. Sep. 2016.

[8] Forti, Adam, Costa, John, Donlon, Elizabeth. "Green Fee Awardee 2017: Designing and Building a Multiple-Rotor Triboelectric Wind Turbine." 2017.

[9] "How Wind Energy Works." Union of Concerned Scientists. Web. Mar. 2017. <http://www.ucsusa.org/clean-energy/renewable-energy/how-wind-energy-works#.WMi6MG_yupo>

Appendices

Appendix A: Triboelectric Series

Table 4: Triboelectric Series for Common Insulators. The metal effect indicates the charge acquired by the material if rubbed with metal, relative to the normal affinity. In this column, N indicates Normal (or consistent with the standard affinity) and W indicates a weak resulting charge affinity. Tests were performed by Bill Lee (Ph.D., physics). ©2009 by AlphaLab, Inc. (TriField.com), which also manufactured the test equipment used. This table may be reproduced only if reproduced in whole [2].

Insulator Name	Affinity (nC/J)	Metal Effect	Notes
Polyurethane foam	+60	+N	All materials are good insulators (>1000 T ohm cm) unless noted.
Sorbothane	+58	-W	Slightly conductive. (120 G ohm cm).
Box sealing tape (BOPP)	+55	+W	Non-sticky side. Becomes more negative if sanded down to the BOPP film.
Hair, oily skin	+45	+N	Skin is conductive. Cannot be charged by metal rubbing.
Solid polyurethane, filled	+40	+N	Slightly conductive. (8 T ohm cm).
Magnesium fluoride (MgF2)	+35	+N	Anti-reflective optical coating.
Nylon, dry skin	+30	+N	Skin is conductive. Cannot be charged by metal rubbing.
Machine oil	+29	+N	
Nylatron (nylon filled with MoS2)	+28	+N	
Glass (soda)	+25	+N	Slightly conductive. (Depends on humidity).
Paper (uncoated copy)	+10	-W	Most papers & cardboard have similar affinity. Slightly conductive.
Wood (pine)	+7	-W	
GE brand Silicone II (hardens in air)	+6	+N	More positive than the other silicone chemistry (see below).
Cotton	+5	+N	Slightly conductive. (Depends on humidity).
Nitrile rubber	+3	-W	
Wool	0	-W	
Polycarbonate	-5	-W	
ABS	-5	-N	
Acrylic (polymethyl methacrylate) and adhesive side of clear carton-sealing and office tape	-10	-N	Several clear tape adhesives are have an affinity almost identical to acrylic, even though various compositions are listed.
Epoxy (circuit board)	-32	-N	
Styrene-butadiene rubber (SBR, Buna S)	-35	-N	Sometimes inaccurately called "neoprene" (see below).
Solvent-based spray paints	-38	-N	May vary.
PET (mylar) cloth	-40	-W	
PET (mylar) solid	-40	+W	

Continued on Next Page

Table 4: Continued

Insulator Name	Affinity (nC/J)	Metal Effect	Notes
EVA rubber for gaskets, filled	-55	-N	Slightly conductive. (10 T ohm cm). Filled rubber will usually conduct.
Gum rubber	-60	-N	Barely conductive. (500 T ohm cm).
Hot melt glue	-62	-N	
Polystyrene	-70	-N	
Polyimide	-70	-N	
Silicones (air harden & thermoset, but not GE)	-72	-N	
Vinyl: flexible (clear tubing)	-75	-N	
Carton-sealing tape (BOPP), sanded down	-85	-N	Raw surface is very + (see above), but close to PP when sanded.
Olefins (alkenes): LDPE, HDPE, PP	-90	-N	UHMWPE is below. Against metals, PP is more neg than PE.
Cellulose nitrate	-93	-N	
Office tape backing (vinyl copolymer?)	-95	-N	
UHMWPE	-95	-N	
Neoprene (polychloroprene, not SBR)	-98	-N	Slightly conductive if filled (1.5 T ohm cm).
PVC (rigid vinyl)	-100	-N	
Latex (natural) rubber	-105	-N	
Viton, filled	-117	-N	Slightly conductive. (40 T ohm cm).
Epichlorohydrin rubber, filled	-118	-N	Slightly conductive. (250 G ohm cm).
Santoprene rubber	-120	-N	
Hypalon rubber, filled	-130	-N	Slightly conductive. (30 T ohm cm).
Butyl rubber, filled	-135	-N	Conductive. (900 M ohm cm). Test was done fast.
EDPM rubber, filled	-140	-N	Slightly conductive. (40 T ohm cm).
Teflon	-190	-N	Surface is fluorine atoms-- very electronegative.

Appendix B: Bill of Materials for Model 3.2

Table 5: Bill of materials for all components of model 3.2. Note that part numbers may not correspond to numbers in figures within the body of the document.

Label	Part Name	Material	Description	Material Source/Part Number	Quantity
1	Narrow Electrode s20 NEF	0.063-inch aluminum sheet	Water Jet by Machine Shop	McMaster Carr/89015K38	1
2	Narrow Electrode s20 WEF	0.063-inch aluminum sheet	Water Jet by Machine Shop	McMaster Carr/89015K38	1
3	PVC s20	0.25-inch polyvinyl chloride (PVC)	Water Jet by Machine Shop	McMaster Carr/8747K126	2
4	Wide Electrode s20 NEF	0.063-inch aluminum sheet	Water Jet by Machine Shop	McMaster Carr/89015K38	1
5	Wide Electrode s20 WEF	0.063-inch aluminum sheet	Water Jet by Machine Shop	McMaster Carr/89015K38	1
6	Electrical Brush	Crimped brass bristles fastened to wire	Manufactured by Hand	Gordon Brush/44775	8
7	Turbine Cap NEF	0.25-inch acrylic	Laser Cut by Engineering Technician	McMaster Carr/8560K355	1
8	Turbine Cap WEF	0.25-inch acrylic	Laser Cut by Engineering Technician	McMaster Carr/8560K355	1
9	Slip Ring Connection Plate NEF	0.25-inch acrylic	Laser Cut by Engineering Technician	McMaster Carr/8560K355	1
10	Slip Ring Connection Plate WEF	0.25-inch acrylic	Laser Cut by Engineering Technician	McMaster Carr/8560K355	1
11	Stand Cap NEF	0.25-inch polycarbonate	Water Jet by Machine Shop	McMaster Carr/8574K43	1
12	Stand Cap WEF	0.25-inch polycarbonate	Water Jet by Machine Shop	McMaster Carr/8574K43	1
13	Test Stand Bar	stainless steel	12-inch threaded rod	Lowe's Home Improvement	4
14	Spacing Washer	0.25-inch acrylic	Laser Cut by Engineering Technician	McMaster Carr/8560K355	12
15	Axial Pipe	Schedule 40 aluminum size 3/8	Machined to spec. by Machine Shop	McMaster Carr/5038K172	2
16	Pipe Bushing	Plastic	Machined to spec. by Machine Shop	Scavenged Scrap	2
17	Ball Bearing	stainless steel	Trade No. R10, for 5/8" Shaft Dia., 1-3/8" OD	McMaster Carr/60355K506	2
18	Slip Ring with Flange	Plastic/wiring	22mm diameter, 6 wires, max 240V @ 2A	Adafruit/736	2
19	Gear Motor	Metal	47:1 Gear Ratio	Pololu/3229	1
20	Motor Bracket	Aluminum Sheet	Purchased with Gear Motor	McMaster Carr/8560K355	1
21	Motor Stand Brace Arm	0.25-inch acrylic	Laser Cut by Engineering Technician	McMaster Carr/8560K355	2
22	Motor Stand Base	0.25-inch acrylic	Laser Cut by Engineering Technician	McMaster Carr/8560K355	1
23	Motor Hub	Aluminum	Contains tapped hole for set screw	Pololu/2676	2
24	Pulley Guard - Motor	0.125-inch laminated wood	Laser Cut by Engineering Technician	Scavenged Scrap	2

Continued on Next Page

Table 5: Continued

| Label	Part Name	Material	Description	Material Source/Part Number	Quantity
25	Pulley Surface - Rotor	0.25-inch acrylic	Laser Cut by Engineering Technician	McMaster Carr/8560K355	2
26	Pulley Guard - Rotor	0.25-inch acrylic	Laser Cut by Engineering Technician	McMaster Carr/8560K355	2
27	Drive Belt	Rubber	Dayco ELA V-Rubber Belt	Dayco/269599 E030195	1
28	Standard Bolt A	stainless steel	0.25-inch dia., 1.25-inch length	Lowe's Home Improvement	6
29	Internal Connecting Rod	stainless steel	5.5-mm dia. threaded rod, 4-inch length	Lowe's Home Improvement	3
30	Standard Nut A	stainless steel	Fit 0.25-inch bolts	Lowe's Home Improvement	22
31	Metric Nut A	stainless steel	Fit 5.5-mm threaded rods	Lowe's Home Improvement	18
32	Motor Stand Bolt	stainless steel	Purchased with Gear Motor	Lowe's Home Improvement	4
33	Motor Stand Nut	stainless steel	Purchased with Gear Motor	Lowe's Home Improvement	4
34	Standard Bolt B	stainless steel	0.25-inch dia., 0.75-inch length	Lowe's Home Improvement	4

Appendix C: Additional Views of Model 3.2
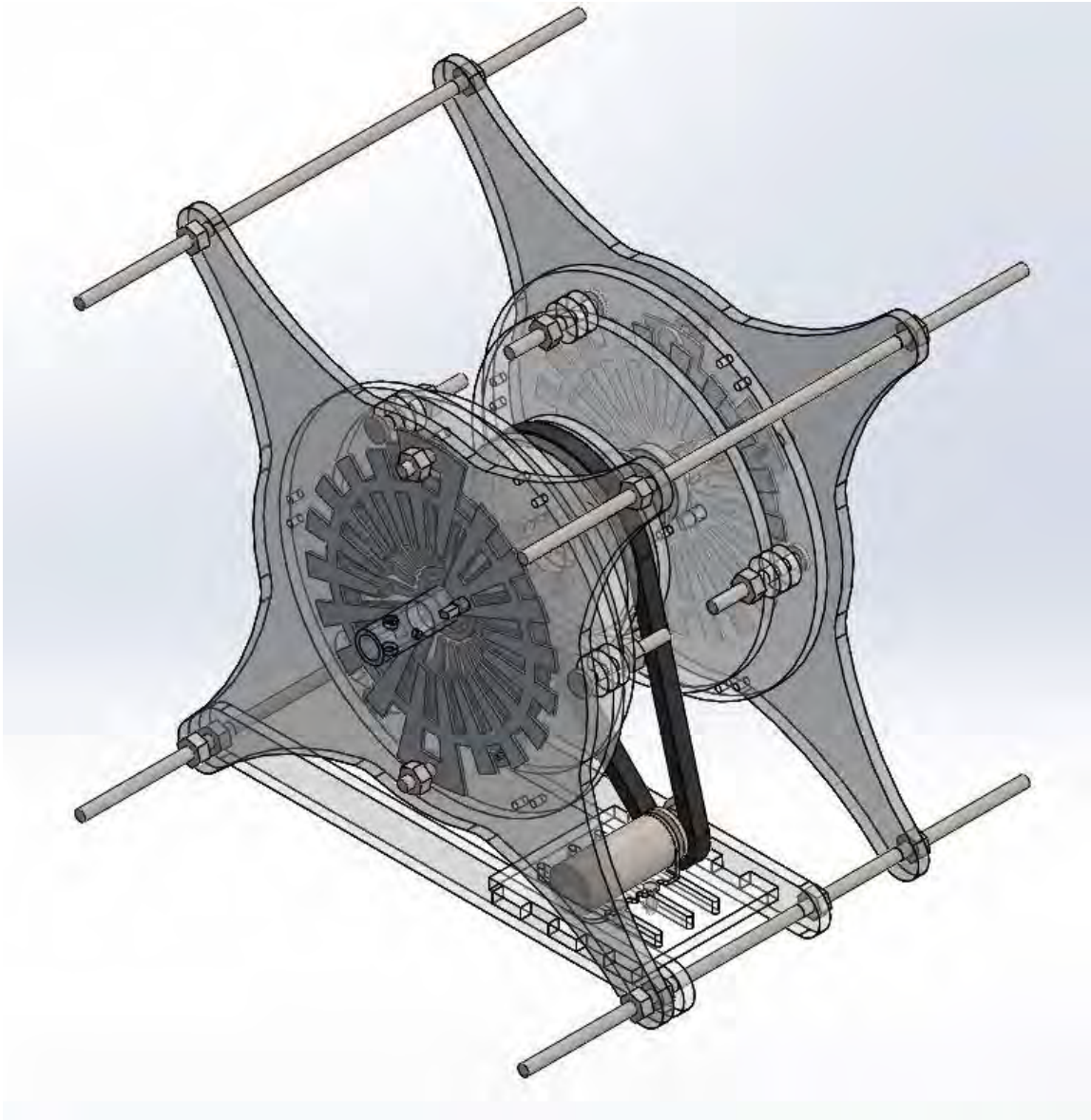
Figure 15: Isometric view of model 3.2, in which the Wide Electrode Fixed (WEF) side is in the foreground. Varying colors and transparencies are the result of SolidWorks materials properties fixed for each component.
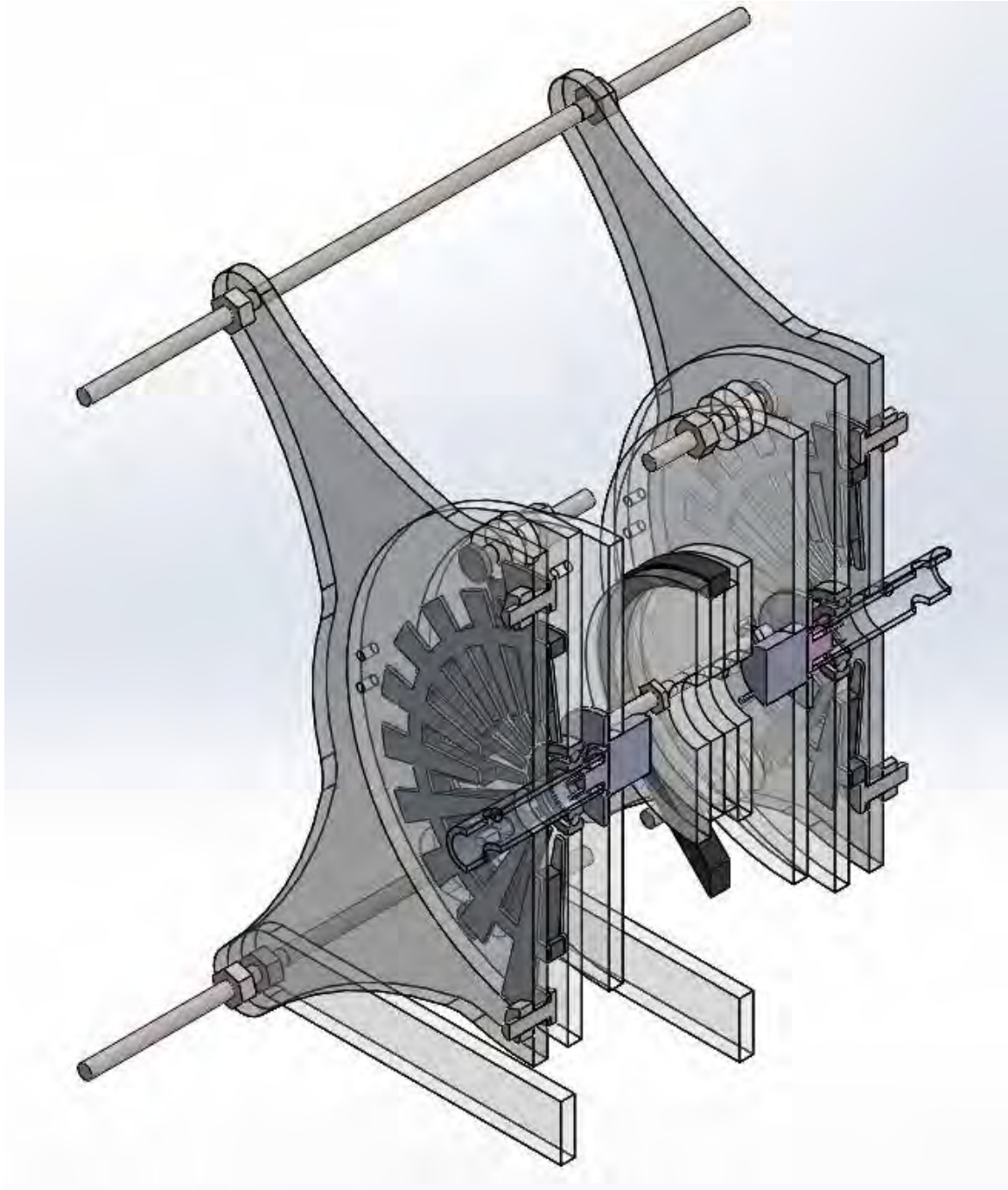
Figure 16: Section of isometric view of model 3.2. Some details of the interior components, such as the pipes and slip rings, are visible.

Appendix D: Wind Energy Approximations

The energy of the wind which impinges upon the wind turbine can be predicted using complicated computer modeling or empirically determined. For purposes of this report, a much simpler approximation is utilized to obtain an estimate, beginning with the definition of kinetic energy:

$$\text{Kinetic Energy} = (1/2) * \text{Mass} * \text{Speed}^2 \qquad\qquad 4$$

This equation is applied to a rectangular prism control volume, containing only air, which has specific dimensions:

$$\text{Length of air} = \text{Wind speed} * \text{Time} \qquad\qquad 5$$

$$\text{Turbine swept area} = \text{Turbine height} * \text{Turbine diameter} \qquad\qquad 6$$

The mass of this air is:

$$\text{Mass} = \text{Air density} * \text{Length of air} * \text{Turbine swept area} \qquad\qquad 7$$

After substituting these equations, for a wind with a given average speed, the kinetic energy it contains may be approximated by Equation 8:

$$\text{Kinetic Energy} = (1/2) * (\text{Air density} * \text{Turbine swept area} * \text{time}) * \text{Wind speed}^3 \qquad\qquad 8$$

Appendix E: Mass Properties of Model 3.2

Table 6: Results of mass properties calculation for the rotating mass in SolidWorks CAD model of turbine model 3.2. In this model, the X axis corresponds to the axis of rotation of the rotor. The mass of all components was estimated by the CAD program upon setting the appropriate material for each component of the assembly.

Mass properties of selected components		
Coordinate system: -- default --		
The center of mass and the moments of inertia are output in the coordinate system of Large Simple Model 03.21		
Mass = 3.16 pounds		
Volume = 59.53 cubic inches		
Surface area = 626.36 square inches		
Center of mass: (inches)		
X = 6.38		
Y = -18.04		
Z = 5.69		
Principal axes of inertia and principal moments of inertia: (pounds * square inches)		
Taken at the center of mass.		
Ix = (0.00, 0.00, 1.00)	Px = 18.86	
Iy = (0.48, -0.88, 0.00)	Py = 21.36	
Iz = (0.88, 0.48, 0.00)	Pz = 21.39	
Moments of inertia: (pounds * square inches)		
Taken at the center of mass and aligned with the output coordinate system.		
Lxx = 21.38	Lxy = -0.01	Lxz = 0.00
Lyx = -0.01	Lyy = 21.37	Lyz = 0.00
Lzx = 0.00	Lzy = 0.00	Lzz = 18.86
Moments of inertia: (pounds * square inches)		
Taken at the output coordinate system.		
Ixx = 1152.32	Ixy = -363.71	Ixz = 114.71
Iyx = -363.71	Iyy = 252.29	Iyz = -324.43
Izx = 114.71	Izy = -324.43	Izz = 1176.07